analytical chemistry

pubs.acs.org/ac Article

Gold Nanoparticle Aggregation-Induced Quantitative Photothermal Biosensing Using a Thermometer: A Simple and Universal Biosensing Platform

Wan Zhou,‡ Kaiqiang Hu,‡ Sharon Kwee, Liang Tang, Zonghua Wang, Jianfei Xia, and XiuJun Li*

Cite This: *Anal. Chem.* 2020, 92, 2739−2747 Read Online

ACCESS | Metrics & More | Article Recommendations | Supporting Information

ABSTRACT: A simple, low-cost, and universal gold nanoparticle (AuNP) aggregation-induced photothermal biosensing platform has been developed for the first time and applied for the visual quantitative genetic detection using a common thermometer. By exploiting the photothermal effect of target-induced gold nanoparticle aggregation, visual quantitative biochemical analysis can be achieved by simply recording temperature signals using a common thermometer. Compared to conventional genetic testing methods, it is label- and amplification-free and can be completed in 40 min without the aid of any advanced analytical instruments. *Mycobacterium tuberculosis* (*MTB*) DNA was used as a model target to demonstrate the application of this photothermal biosensing platform. Although no costly instrument was used, high sensitivity and specificity were achieved with the limit of detection (LOD) of 0.28 nM, which was nearly 10-fold lower than that of the colorimetric method using a spectrometer. This AuNP aggregation-induced photothermal biosensing strategy provides a simple, low-cost, and universal platform for broad application of visual quantitative detection of nucleic acids and many other biomolecules, particularly in point-of-care (POC) biosensing applications.

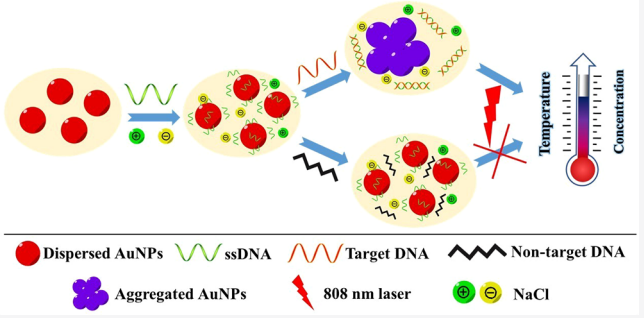

Quantitative and sensitive genetic analysis techniques play a crucial role in numerous fields involved in clinical diagnostics,[1−4] forensic science,[5] drug development,[6] food safety surveillance,[7] and environmental monitoring.[8,9] A number of DNA detection methods have been developed including colorimetry,[10−13] fluorescence,[14−17] chemiluminescence,[18,19] and electrochemistry.[20−22] However, most methods still require bulky and costly instruments. Among all detection methods, nanomaterial-based colorimetric assays, especially using gold nanoparticles (AuNPs)-based biosensors have been the most commonly used detection method due to the unique surface plasmon resonance (SPR) absorption of AuNPs, simple operation, and distinct color changes.[11,23−26] However, most colorimetric methods pose the issue of low detection sensitivity and are not suitable for quantitative detection unless using specialized instruments (e.g., microplate reader).

Conventional nucleic acid detection methods mainly consist of nucleic acid amplification-based methods,[27,28] such as polymerase chain reaction (PCR)[5,23] and DNA hybridization-based techniques (e.g., DNA microarray).[1,29] These conventional nucleic acid detection methods largely require two functionalization processes: (1) specific functionalization of AuNPs (or some other nanomaterials) mostly with −SH functional groups and (2) functionalization of DNA products/primers/probes with other functional groups, such as $-NH_2$, to link with AuNPs, or some fluorescence fluorophores (e.g., fluorescein amidite (FAM), Cy3, Cy5, Cy7, etc.) for the purpose of detection,[1] all of which make the entire detection methods costly, cumbersome, and time-consuming. Moreover, one DNA-functionalized nanosensor is usually limited to one target; changing to a different target relies on a new round of nanoparticle functionalization. Accordingly, such peculiar recognition, amplification, and detection mechanisms pose limits for versatile broad applications in detecting different DNA sequences. Hence, there has been an increasing interest in the development of a universal platform integrated with label-free and DNA amplification-free biosensing mechanisms for quantitative DNA detection at the point of care.

Photothermal (PT) effect has been extensively studied and applied in cancer therapy because of the unique photothermal conversion property of photothermal agents,[30] involving in gold-based nanomaterials,[31−33] carbon-based nanomaterials,[34,35] and organic molecule dyes.[36,37] Recently, new applications of photothermal agents have been explored, in

Received: November 2, 2019
Accepted: January 15, 2020
Published: January 24, 2020

https://dx.doi.org/10.1021/acs.analchem.9b04996
Anal. Chem. 2020, 92, 2739−2747

which nanomaterials-based photothermal biosensing emerged as a novel and attractive method in the quantitative detection of biomolecules. Our group, for the first time, developed a new photothermal immunoassay platform for the quantitative detection of protein-based cancer biomarkers using an inexpensive thermometer,[38] followed with a few other photothermal immunosensing platforms.[39] For example, by introducing different photothermal probes, such as Prussian blue nanoparticles (PB NPs)[38,40] and small organic molecules (i.e., oxidized 3,3′,5,5′-tetramethylbenzidine or oxidized TMB),[39] the target information on disease biomarkers was converted into photothermal signals (i.e., temperature changes) and, thus, was quantitatively measured simply by using a household thermometer. As compared to the conventional enzyme-linked immunosorbent assay (ELISA),[41] which is based on colorimetric detection, the photothermal immunoassay is superior as it provides a simple, low-cost, and quantitative detection platform, in which no costly and bulky analytical instrument or trained personnel is needed, with minimal color interference. Unfortunately, most photothermal biosensing platforms target protein-based biomarkers, there are few reports to develop new photothermal biosensing platforms for genetic analysis.

Herein, we developed a new simple and universal method for quantitative genetic analysis using a thermometer on the basis of AuNP aggregation-induced photothermal effects. In this method, two competing processes were present between the protection and the destabilization of dispersed AuNPs by single-stranded DNA (ssDNA) probes and salt, respectively. When adding target DNA, ssDNA probes were deprived of the surface protection of AuNPs because of the hybridization, promoting AuNPs to change from the dispersed status to the aggregated status. The obtained AuNP aggregation was used as a novel photothermal biosensor, correlating quantitative analysis of nucleic acids with temperature readouts, which could be simply recorded by using a common thermometer. With this strategy, there is no need for DNA amplification, surface modification of AuNPs, and ssDNA probe modification, which greatly reduces the complexity and cost of genetic assays. The entire assay can be accomplished within 40 min using only a thermometer as a signal reader, without the assistance from any bulky and costly instrumentation. In addition, the unmodified AuNPs can be used to adsorb various DNA probes, making it a universal platform for a broad range of genetic targets. By using *Mycobacterium tuberculosis* (*MTB*) DNA as a model target, high sensitivity and specificity were achieved with the limit of detection (LOD) as low as 0.28 nM, which was nearly 10-fold lower than that in the colorimetric method using a microplate reader. To the best of our knowledge, this is the first photothermal biosensing system for quantitative genetic analysis using a thermometer, and it is also the first time to apply AuNP aggregation in a photothermal biosensing platform for quantitative DNA detection.

EXPERIMENTAL SECTION

Reagents and Materials. Gold nanoparticles (AuNPs, 20 nm in diameter), saline-sodium citrate (SSC) buffer (20× concentrate, 3 M NaCl, pH 7.0), and normal human serum were purchased from Sigma (St. Louis, MO, US). All oligonucleotide sequences were produced from Integrated DNA Technologies (Coralville, IA, US) and listed in Table S1. Genomic DNA sequences were extracted from *Mycobacterium tuberculosis* (*M. tuberculosis*), *Bordetella pertussis* (*B. pertussis*), *Escherichia coli* (*E. coli*), MCF-7 cells based on previously published protocols.[2,4,42] All chemicals were used as received without further purification and Milli-Q water (18.2 MΩ·cm) was used from a Millipore system (Bedford, MA, US) unless otherwise noted.

Condition Optimization. In the optimization of salt (NaCl) concentration in the photothermal biosensing platform, 20 μL of NaCl at different concentrations in SSC buffers (3× SSC, 5 mM trisodium citrate) was added to bare AuNP suspensions (1.2 nM) with the final concentration from 0 to 100 mM. In the optimization process of ssDNA probe concentration, 20 μL of ssDNA probes at different concentrations in SSC buffer were added to bare AuNP suspensions (1.2 nM) with the final concentration from 0 to 320 nM, followed by the addition of 40 mM NaCl in SSC buffer.

UV−vis spectroscopic characterization of the above suspensions was carried out on a microplate reader (Molecular Devices, LLC, Sunnyvale, CA, US) using a 96-well microplate. SEM images were taken on a Hitachi S5500 scanning transmission electron microscope. In the photothermal testing, an 808 nm diode laser (Model MDL-III-808, Opto Engine, Midvale, UT, US) was used to irradiate AuNP suspensions. Temperature change of each suspension (200 μL) was recorded using a common digital thermometer or a dual input type J/K digital thermometer (Model 421502, Extech Instruments Corporation, US) immediately after laser irradiation for 5 min at the power density of 5.2 W/cm^2. In the optimization of the laser irradiation time, the kinetic temperature increase was recorded every 30 s and up to 10 min under the continuous laser irradiation at the power density of 5.2 W/cm^2. The position of the thermometer probe was fixed in all temperature measurements to avoid temperature variations from position to position, with the distance of 0.8 cm from the bottom of detection tubes.

Procedures of Quantitative Photothermal Biosensing Using a Thermometer. Under optimal conditions, the photothermal biosensing platform based on AuNP aggregation was applied for the quantitative detection of the target *MTB* DNA. The target *MTB* DNA with varying concentrations from 0 to 1200 nM was added to ssDNA probes (160 nM) protected AuNP suspensions and incubated at 37 °C for 30 min. With the addition of NaCl (40 mM), the temperature of each suspension (200 μL) was recorded immediately after the laser irradiation for 8 min at the power density of 5.2 W/cm^2. Three other types of different nucleic acids (both probes and targets), including *Neisseria meningitidis* (*N. meningitidis*), miRNA-141, and *Giardia lamblia* (*G. lamblia*), were also chosen to test the universality and wide applications of the method, with the probe concentration and the target concentration of 160 and 50 nM, respectively, followed by the same hybridization and detection procedures as the aforementioned.

In the specificity test, genomic DNA was extracted from *M. tuberculosis*, *B. pertussis*, *E. coli*, and MCF-7 breast cancer cells based on previous protocols.[1,2,43] Prior to the hybridization step, the genomic DNA was first denatured at 95 °C for 10 min, followed by being placed on ice for 1 min. Genomic DNA was then used in a similar procedure as the above-mentioned.

https://dx.doi.org/10.1021/acs.analchem.9b04996
Anal. Chem. 2020, 92, 2739−2747

RESULTS AND DISCUSSION

Working Principle of AuNP Aggregation-Induced Photothermal Biosensing Platform and Feasibility Tests. As illustrated in Scheme 1, the working principle is built on the PT effect difference of AuNPs in different statuses—dispersed AuNPs have a weak PT effect, while aggregated AuNPs have a much stronger PT effect. The AuNP aggregation is mainly due to the adsorption disparity onto AuNPs between ssDNA and double-stranded DNA (dsDNA) after adding high concentrations of salt.[44] It was reported that the disparity in adsorption onto unmodified AuNPs exists between ssDNA probes and dsDNA.[45] Specifically, ssDNA probes are able to be adsorbed onto AuNPs via van der Waals attraction between the exposed bases and the gold surface. However, dsDNA has little affinity to AuNPs because of its stable double-helix geometry that inhibits the exposure of nucleobases and leads to the electrostatic repulsive interaction between the negatively charged phosphate backbone and AuNPs.[24,46,47] Therefore, in this work, unmodified AuNPs are first protected by ssDNA probes from salt-induced aggregation, which are in the dispersed status and have weak PT effect under the irradiation of a near-infrared (NIR) laser. In the presence of target DNA, the protection is damaged due to DNA hybridization, which causes the aggregation of AuNPs upon the addition of salt. The AuNP aggregation is formed and used as a photothermal agent for photothermal biosensing. As such, an obvious temperature increase can be obtained from the aggregated AuNP suspension while being irradiated by the NIR laser. However, AuNPs remain in dispersed status while adding nontarget DNA, which causes a negligible temperature increase due to a weak PT effect. Therefore, DNA quantification can be achieved by simply recording the temperature change by using a thermometer.

The feasibility of this photothermal biosensing platform was first investigated by testing absorption spectra and PT effects of different components in this platform. Different solutions were characterized by UV−vis spectra (Figure 1A), photothermal testing (Figure 1B), and scanning electron microscopy (SEM, Figure 1C), including (a) SSC buffer as the blank, (b) bare AuNP suspension, (c) AuNP suspension upon the addition of NaCl in a SSC buffer, and (d−e) ssDNA probe-protected AuNP suspensions upon the addition of salt (40 mM) in SSC buffers in the absence (d) and presence of (e) target DNA (with the concentration of 1600 nM). The PT effect of different components was studied by measuring temperature changes (ΔTs) of all the above solutions after the irradiation of NIR laser for 5 min at a power density of 5.2 W/cm^2. Figure 1 shows that bare AuNPs (suspension b) remained red in color, while the typical absorption peak was 520 nm (Figure 1A) with SSC buffer as blank (a). The bare AuNPs (with a diameter of 20 nm) were in dispersed status according to the SEM image in Figure 1C (b). No obvious temperature increase was obtained under the laser irradiation. However, by adding salt, the color of AuNPs (suspension c) changed to blue and a peak at 750 nm appeared due to red shift of the SPR peak, which was resulted from AuNP aggregation (Figure 1C (c)). In addition, a dramatic temperature increase of ∼13 °C was obtained under laser irradiation. Conversely, when adding ssDNA probes, with the adsorption of ssDNA on the surface, AuNPs (suspension d) were protected and no obvious changes were observed in UV−vis spectra, SEM image (Figure 1C (d)), and temperature measurement. However, in the presence of target DNA, the hybridization of ssDNA probes and target DNA led to AuNPs unprotected and aggregated when adding salt (suspension e). The color of suspension changed from red to purple/blue and a shoulder peak centered at around 650 nm appeared, which was mainly due to DNA hybridization and AuNP aggregation (Figure 2C (e)). An obvious temperature increase of ∼11 °C was recorded in suspension e under the laser irradiation, which implied temperature signals could be used as readouts for biosensing. The results proved it is feasible to apply target DNA-induced AuNP aggregation for the photothermal biosensing using a thermometer.

Scheme 1. Schematic Illustration of the Principle of AuNP Aggregation-Induced Photothermal Biosensing of Target DNA Using a Thermometer

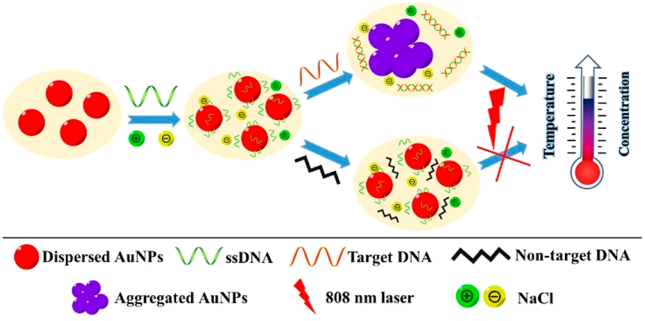

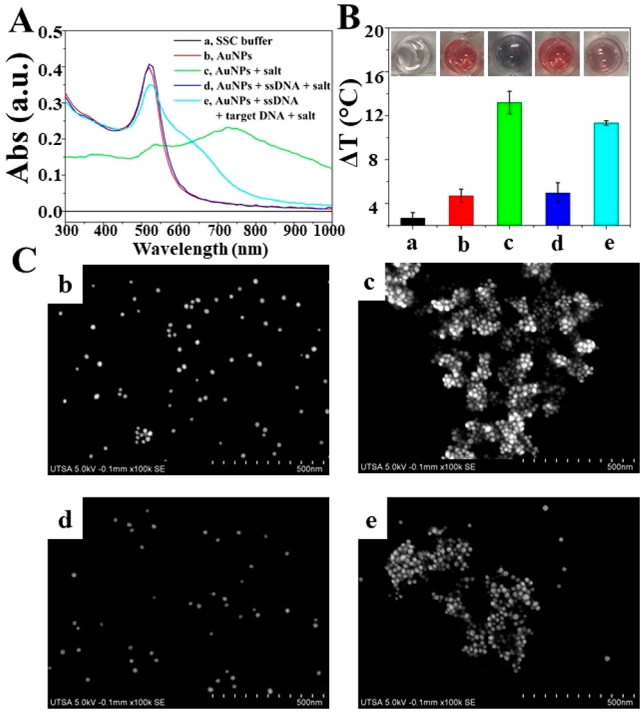

Figure 1. Feasibility tests of the AuNP aggregation-induced photothermal biosensing. (A) UV−vis spectra and (B) temperature changes of different suspensions including (a) SSC buffer as blank, (b) dispersed AuNP suspension (1.2 nM), (c) AuNPs + salt (40 mM) in a SSC buffer, (d) AuNPs + ssDNA (320 nM) + salt (40 mM), and (e) AuNPs + ssDNA (320 nM) + target DNA (1600 nM) + salt (40 mM). Insets in panel B are photographs of suspensions a−e (from left to right). (C) SEM images of different suspensions of b−e. The power density of the 808 nm NIR laser was 5.2 W/cm^2, and the irradiation time was 5 min. Error bars represent standard deviations (n = 3).

https://dx.doi.org/10.1021/acs.analchem.9b04996
Anal. Chem. 2020, 92, 2739−2747

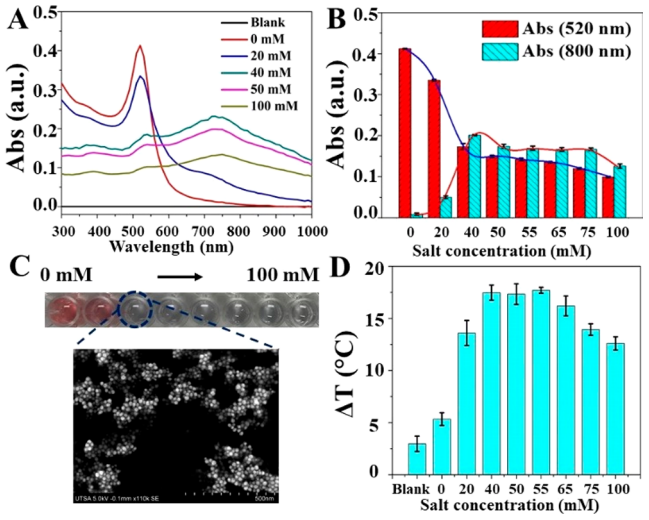

Figure 2. Optimization of salt concentrations in the AuNP aggregation-induced photothermal biosensing method: (A) UV−vis spectra, (B) absorbances at 520 and 800 nm, and (C) photographs of AuNP suspensions upon the addition of salt with the final concentration ranging from 0 to 100 mM. The inset in panel C is the SEM image of AuNP suspension after the addition of 40 mM salt. (D) Temperature increases of the above AuNP suspensions under 808 nm laser irradiation. The laser power density was 5.2 W/cm^2, and the irradiation time was 5 min. SSC buffer was used as blank. Error bars represent standard deviations (n = 3).

Condition Optimization. In this photothermal biosensing system, different factors can significantly affect the detection performance, such as concentrations of salt (NaCl) and ssDNA probes and laser irradiation time. Therefore, we further optimized the above conditions in the following experiments. In the UV−vis spectra, absorbance at 520 nm was used to study the AuNPs dispersed status, while absorbance at 800 nm was chosen to study the photothermal effect of aggregated AuNPs in the NIR range.

The concentration of salt (NaCl) was first optimized because of its key role in causing AuNP aggregation, resulting in a strong PT effect. Different concentrations of NaCl were added to bare AuNP suspensions with the final salt concentrations ranging from 0 to 100 mM. The AuNP suspensions were characterized by UV−vis spectroscopy, photothermal effects, and SEM, and the results were shown in Figure 2. It can be seen that the color of AuNP suspensions changed from red to purple/blue (Figure 2C) with the increase of salt concentrations, indicating changes in the surface charge of AuNPs, which led to the aggregation.[44,48,49] This phenomenon was further proved by UV−vis characterization in Figure 2A. With the increase of salt concentrations, along with the peak at 520 nm, a second peak at a longer wavelength around 750 nm appeared due to the formation of aggregates, indicating stronger photothermal effects in the NIR range. Moreover, as shown in Figure 2B, the absorbances at 520 nm decreased sharply at the salt concentrations of 0−40 mM owing to the depletion of dispersed nanoparticles and then reached a plateau when the concentration was higher than 40 mM because of the complete formation of aggregated nanoparticles. In contrast, absorbances at 800 nm (Figure 2B) increased when increasing the salt concentrations from 0 to 40 mM and reached a plateau at concentrations higher than 40 and up to 100 mM, while the SEM image in Figure 2C confirmed the aggregated status of AuNPs at the salt concentration of 40 mM. The optical absorption changes at 800 nm further proved the transformation of dispersed nanoparticles to aggregated nanoparticles when increasing the concentration of NaCl, which also suggested the changes from weak PT effects to strong PT effects, as confirmed by Figure 2D. Under the irradiation of a NIR laser, the temperature first increased rapidly upon adding salt in the concentration range from 0 to 40 mM, then reached a plateau ($\Delta T \sim 18$ °C) in the concentration range of 40−65 mM, and slightly decreased afterward. This was mainly caused by more aggregated AuNPs formed when adding salt to bare AuNP suspensions. Moreover, upon the addition of excess salt (i.e., higher than 40 mM), the aggregated AuNPs further accumulated and started to precipitate, which caused lower signals in both absorbances at 800 nm and temperature measurement. Therefore, 40 mM of salt was selected as the optimal concentration and used in the following experiments.

To obtain the best protection performance of AuNPs by oligonucleotides, the concentration of ssDNA probes was then optimized. Different concentrations of ssDNA probes in the range of 0−320 nM were added to AuNP suspensions, followed by the addition of 40 mM NaCl. Figure 3 shows the

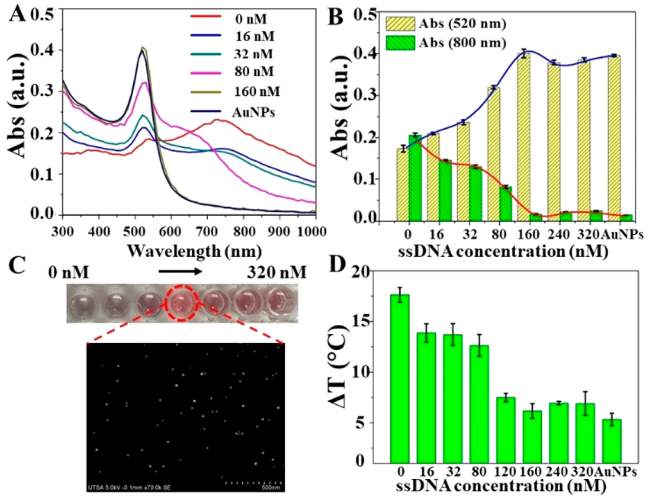

Figure 3. Optimization of ssDNA concentrations in the AuNP aggregation-based photothermal biosensing method: (A) UV−vis spectra, (B) absorbances at 520 and 800 nm, and (C) photographs of AuNP suspensions with ssDNA protection in the final concentration range of 0−320 nM in the presence of 40 mM salt. The inset in panel C is the SEM image of the ssDNA (160 nM) protected AuNP suspension in the presence of 40 mM salt. (D) Temperature increases of the above AuNP suspensions under the 808 nm laser irradiation. The laser power density was 5.2 W/cm^2, and the irradiation time was 5 min. Error bars represent standard deviations (n = 3).

UV−vis spectra, photographs, SEM characterization, and temperature measurements of the above suspensions. Color changes from purple/blue to red were observed with the increase of ssDNA probe concentrations in Figure 3C, representing the changes of surface charges and the status of nanoparticles. It can be seen from Figure 3A that the peak at a longer wavelength around 750 nm became weaker until disappeared when adding higher concentrations of ssDNA probes, indicating the depletion of aggregated AuNPs and better ssDNA protection. In addition, as shown in Figure 3B, the absorbances at 520 nm increased gradually in the

https://dx.doi.org/10.1021/acs.analchem.9b04996
Anal. Chem. 2020, 92, 2739−2747

concentration range from 0 to 160 nM, implying the formation of dispersed AuNPs due to increased ssDNA probe protection. When the concentration was higher than 160 nM (e.g., 320 nM), no obvious change in UV−vis spectra was observed as compared to bare AuNPs (Figure S1), indicating that the maximum protection of AuNPs can be achieved at the ssDNA concentration of 160 nM. Moreover, the absorbance at 520 nm reached the highest value at the concentration of 160 nM, which was almost the same as the bare AuNPs, suggesting that the dispersed status of nanoparticles (as seen in the SEM image in Figure 3C) was recovered from salt-induced aggregation by the protection of ssDNA probes. In contrast, absorbances at 800 nm decreased when increasing the ssDNA probe concentrations from 0 to 160 nM and reached the lowest value at 160 nM, indicating the depletion of aggregated nanoparticles as well as weaker PT effects. Furthermore, under the irradiation of a NIR laser, the temperature increased dramatically up to ΔT of ∼18 °C (Figure 3D) with no addition of ssDNA probes owing to the strong PT effect of AuNP aggregation. Temperature signals decreased with the increase of ssDNA probes concentration until reaching a plateau (ΔT of ∼6 °C) at the final concentration of 160 nM, similar to bare AuNPs. The weaker PT effects of the suspensions indicated that AuNPs were protected from salt-induced aggregation by the addition of ssDNA probes. Conclusively, with the increase of ssDNA probes concentration, more AuNPs remained in the dispersed status in the suspension, which finally reached the initial bare AuNPs status. Therefore, 160 nM of ssDNA was selected as the optimal concentration and used in the following experiments.

The irradiation time in the AuNP aggregation-based photothermal biosensing was also optimized prior to the detection of target DNA, because it could significantly affect the measurement of readout signals (i.e., temperature). By using the optimal concentrations of ssDNA probes and salt, the kinetic temperature increases of different suspensions were recorded every 30 s from 0 to 10 min, including SSC buffer as blank, bare AuNP suspension, aggregated AuNP suspension upon the addition of 40 mM NaCl, and ssDNA (160 nM) protected AuNP suspension upon the addition of 40 mM NaCl. The results in Figure 4 shows that under the continuous irradiation of a NIR laser, the temperature of the aggregated AuNP suspension increased dramatically in the first 2.5 min, then exhibited a stagnant increase, and finally reached the plateau (ΔT of ∼14 °C) at approximately 8 min, where the heat balance was achieved between heat generation from the photothermal effect and heat dissipation to the environment. In contrast, only a slight temperature increase of ∼2 °C was recorded from the blank (SSC buffer), while a temperature increase of ∼4 °C occurred to bare AuNPs and ssDNA probes protected AuNPs in the presence of salt. Therefore, to acquire a stable and sensitive temperature measurement, the laser irradiation time of 8 min was selected as the optimal irradiation time and used in the following experiments.

Quantitative Genetic Analysis of Target DNA with a Thermometer on the Photothermal Biosensing Platform. Under optimal conditions, quantitative photothermal biosensing of target DNA could be achieved by simply monitoring the temperature changes of AuNP suspensions using a thermometer. Tuberculosis (TB) caused by the bacillus *Mycobacterium tuberculosis* (*MTB*) has been one of the deadliest "big 3" infectious diseases,[50] resulting in around 1.5 million deaths annually, particularly in low-income countries.

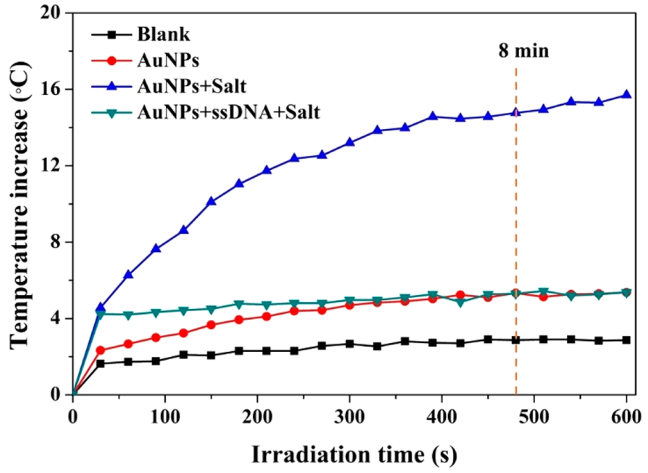

Figure 4. Optimization of the irradiation time in the photothermal biosensing method. Temperature increases versus irradiation time in the range of 0−600 s under the 808 nm laser irradiation from different suspensions: SSC buffer as blank, AuNP suspension, aggregated AuNPs + 40 mM salt, and AuNPs + 160 nM ssDNA + 40 mM salt (under optimal conditions). The laser power density was 5.2 W/cm^2.

Various detection methods targeting *MTB* DNA have been developed including colorimetry,[51,52] electrochemistry,[53] fluorescence,[54] and chemiluminescence.[55] However, most of these methods require complicated DNA amplification procedures, sophisticated infrastructure, and well-trained personnel, which significantly lead to the high cost of TB diagnosis and limit their accessibility in low-resource settings. In this work, we chose *MTB* DNA as a model target to demonstrate the application of the novel AuNP aggregation-based photothermal biosensing in genetic analysis using a common thermometer, with no assistance from any DNA amplification process or expensive instruments.

We first studied UV−vis spectra to characterize this platform for quantitative biosensing using a microplate reader. Target *MTB* DNA with varying concentrations of 0−1200 nM was added to different ssDNA probes (160 nM) protected AuNP suspensions, followed by the addition of NaCl (40 mM). As shown in Figure 5A, with the addition of target DNA, a shoulder peak at around 650 nm to the NIR range appeared and increased with the increase of *MTB* DNA concentrations, while absorbances at 520 nm decreased. The result can be

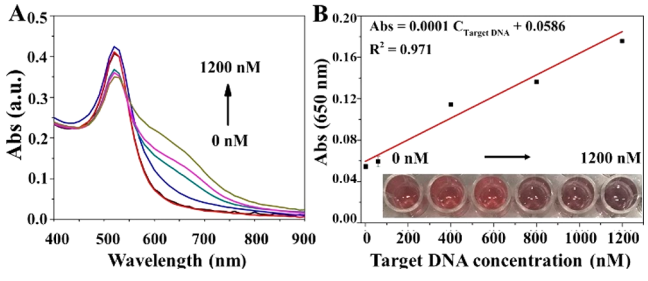

Figure 5. UV−vis characterization of the photothermal biosensing system for quantitative genetic analysis and colorimetric detection of *MTB* DNA using a microplate reader. (A) UV−vis spectra and (B) calibration curve of absorbance at 650 nm with photographs (inset) of target DNA-induced AuNP aggregation suspensions upon the addition of target *MTB* DNA with different concentrations of 0, 4, 60, 400, 800, and 1200 nM (from left to right). Error bars represent standard deviations (n = 3).

https://dx.doi.org/10.1021/acs.analchem.9b04996
Anal. Chem. 2020, 92, 2739−2747

attributed to the speculation that more ssDNA probes were hybridized with the target DNA. When more protection ssDNA probes were consumed, the protection to AuNPs was impaired. As such, more AuNPs aggregated upon the addition of NaCl, which was consistent with the color change from red to purple/blue in Figure 5B. Moreover, it is worthy to note that the absorbances at 650 nm were proportional to the concentration of the target DNA and a linear relationship (Figure 5B) was obtained in the concentration range from 4 to 1200 nM, with the slope of 0.0001 nM^{-1}, indicating the feasibility for quantitative bioanalysis using the AuNP aggregation-induced photothermal biosensing method with a thermometer. The limit of detection (LOD) was calculated based on three folds standard deviation above the blank and determined to be 2.0 nM, whereas the colorimetric detection requires a spectrometer (i.e., the microplate reader).

We then studied the target-induced AuNP aggregation-based photothermal biosensing platform for quantitative detection of *MTB* DNA using a thermometer. The above suspensions added with different concentrations of the target *MTB* DNA were irradiated by a NIR laser (808 nm) for 8 min at the power density of 5.2 W/cm^2, and the temperature was recorded immediately using a portable digital thermometer after the irradiation. The results in Figure 6A exhibit that the temperature increased with the increase of target DNA concentration. There was a linear relationship obtained between the temperature increase with the logarithm of target *MTB* DNA concentration in the range from 2 to 1200 nM, with a squared correlation coefficient of 0.996. The LOD was calculated to be 0.28 nM based on three folds standard deviation above the blank, which was about 10-fold lower than that obtained from our colorimetric detection method, indicating high detection sensitivity of this photothermal biosensing method. Moreover, as compared to conventional colorimetric methods, the proposed photothermal biosensing platform is simple and convenient for quantitative analysis simply using an inexpensive thermometer as a signal reader, whereas conventional colorimetric methods require the use of expensive spectrometers for quantitative analysis. It is worthy to note that although an inexpensive thermometer is used as the signal reader, the sensitivity is even higher than those previously reported one (e.g., reported LODs = 2.5,[56] 2.6,[57] 10.4,[58] and 33 nM,[59]). Furthermore, no DNA amplification was needed, and the detection could be completed within 40 min with no assistance from analytical instrumentation, which greatly reduced the complexity, cost, and detection time of the entire assay.

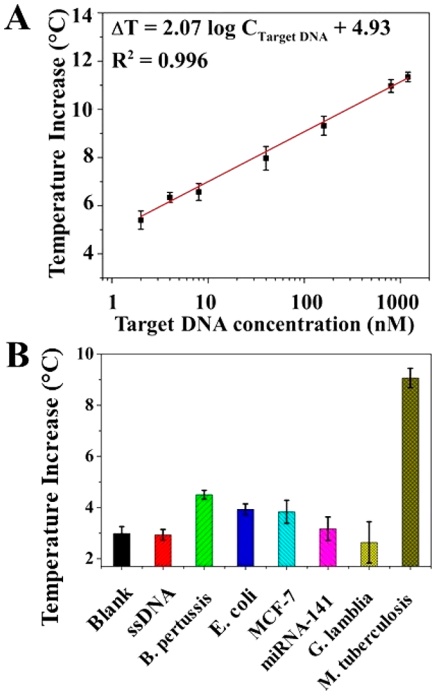

Figure 6. Quantitative genetic analysis of *MTB* on the AuNP aggregation-based photothermal biosensing platform using a thermometer. (A) Calibration curve of temperature increases vs target *MTB* DNA logarithmic concentrations in the range of 2−1200 nM. (B) Specificity test using different interfering nucleic acids on the photothermal biosensing platform, that is, temperature increases of AuNP suspensions upon the addition of *M. tuberculosis* target genomic DNA (39 nM) vs different interfering substances at 3-fold higher concentrations including SSC buffer as blank, ssDNA, genomic DNA extracted from *B. pertussis*, *E. coli*, and MCF-7 cells, miRNA-141, and *G. lamblia* DNA. The laser (808 nm) power density was 5.2 W/cm^2, and the irradiation time was 8 min. Error bars represent standard deviations (n = 3).

The specificity of the AuNP aggregation-induced photothermal biosensing assay was then investigated. Various nucleic acids including genomic DNA sequences extracted from *B. pertussis*, *E. coli*, and breast cancer cells (MCF-7), cancer-associated miRNA (miRNA-141), and parasitic infections-related *G. lamblia* DNA, were used in the assay as interfering substances at 3-fold higher concentrations, in addition to the target *M. tuberculosis* genomic DNA. UV−vis characterization using absorbances at 650 nm and photothermal biosensing using temperature as readouts were studied and the results were shown in Figures S2 and 6B, respectively. Only upon the addition of the target *M. tuberculosis* DNA, an obvious absorbance at 650 nm (Figure S2) appeared with a dramatic temperature increase of ∼9 °C (Figure 6B), while other samples with the addition of ssDNA, *B. pertussis*, *E. coli*, and MCF-7 cells extracted genomic DNA, miRNA-141, and *G. lamblia* DNA had no apparent temperature change as compared to the SSC buffer as blank. More than 200% higher temperature increases were still obtained when detecting target *M. tuberculosis* genomic DNA at a 3-fold lower concentration compared to other nucleic acids. The results demonstrated high specificity of our photothermal biosensing platform for quantitative genetic analysis even in the presence of higher concentrations of interfering substances.

To further demonstrate wide applications and universality of this photothermal biosensing platform in genetic analysis, we tested a few other nucleic acids using this method including *N. meningitidis*, miRNA-141, and *G. lamblia*. Basically, three pairs of these protection probes and their complementary targets were tested, following the optimal experimental procedures. As seen in Figure 7, distinctive increases of temperature (>10 °C) were obtained in all three targets, compared with the blank, indicating wide application of this universal photothermal biosensing platform.

The analytical performance of this photothermal biosensing platform was investigated by testing recovery in the quantitation of *M. tuberculosis* genomic DNA. The analytical recovery was evaluated by spiking different concentrations of target *M. tuberculosis* genomic DNA. Color images of different samples were captured, and temperature increases were recorded immediately after the laser irradiation. The results

https://dx.doi.org/10.1021/acs.analchem.9b04996
Anal. Chem. 2020, 92, 2739−2747

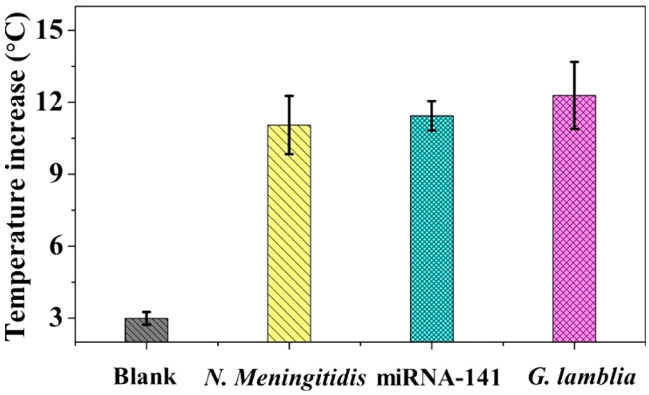

Figure 7. Detection of various target nucleic acids (*N. meningitidis* DNA, miRNA-141, and *G. lamblia* DNA) using the photothermal biosensing platform. All tests were performed under optimal conditions with all complementary probes and targets at the same concentration of 160 nM and 50 nM, respectively. Error bars represent standard deviations (n = 3).

were summarized in Table 1. The analytical recoveries were obtained from 94.5 to 110.2% when testing varying

Table 1. Analytical Performance of the Photothermal Biosensing Platform for *M. tuberculosis* Genomic DNA Detection

Sample No.	Spiked target concentration (μg/mL)	Spiked target concentration (nM)	Color images	PT biosensing detected concentration (μg/mL)	Recovery (%)
Control (SSC buffer)	0	0			
1	2.5	13		2.4	94.5 ± 8.6
2	5.0	27		4.7	94.6 ± 3.9
3	7.5	39		8.3	110.2 ± 4.3
Control (50% serum)	0	0			
4	9.6	50		8.8	91.5 ± 3.9

concentrations of the target genomic DNA spiked in SSC buffer (samples 1−3) from 13 to 39 nM (i.e., 2.5−7.5 μg/mL), which were within the acceptable recovery range for the validation of bioanalytical methods.[60] Besides, although genetic assays usually require cell lysis and DNA extraction before DNA hybridization under optimal hybridization conditions, this platform was also challenged by directly spiking target DNA in a 50% normal human serum sample (sample 4).[61,62] The acceptable analytical recovery of 91.5% was acquired, which further demonstrated the excellent performance of this method even in a complex matrix. Furthermore, as compared to color changes observed by the naked eye, the photothermal biosensing based on target-induced AuNP aggregation provided a simple yet reliable platform for the quantitative detection of nucleic acids.

CONCLUSION

We, for the first time, developed a simple yet versatile AuNP aggregation-induced photothermal biosensing platform for sensitive and quantitative detection of nucleic acids using a thermometer. The quantitation detection can be achieved by simply using a thermometer as the signal reader with no assistance from any specialized and costly analytical instrumentation. Although a low-cost thermometer was used as the signal reader, high sensitivity was achieved with the LOD as low as 0.28 nM, about 10-fold lower than the LOD in the colorimetric detection method using a spectrometer. Moreover, it is a universal platform for DNA detection, as labeling of DNA probes, AuNPs, or DNA amplification processes are not required, which greatly reduces the complexity and cost of detection assays. Furthermore, this photothermal biosensing platform also provides unprecedented potential for the quantitative detection of a wide range of biochemicals and biological organisms, not solely nucleic acids. For instance, by using DNA-based aptamers, this platform can be applied to detect a variety of chemicals ranging from protein biomarkers,[63] microorganisms,[64] cancer cells,[29] to metal ions (e.g., Hg^{2+}).[65] Considering more and more inexpensive portable yet powerful NIR laser pointers become commercially available, this novel biosensing method will bring a new horizon to conventional detection methods particularly for point-of-care testing (POCT).

ASSOCIATED CONTENT

Supporting Information

The Supporting Information is available free of charge at https://pubs.acs.org/doi/10.1021/acs.analchem.9b04996.

DNA sequences used in the photothermal biosensing platform, UV−vis spectra of bare AuNPs and AuNP suspensions with ssDNA protection, and absorbances at 650 nm of AuNP suspensions in detection of target DNA and interfering substances (PDF)

AUTHOR INFORMATION

Corresponding Author

XiuJun Li − *Department of Chemistry and Biochemistry, Biomedical Engineering, Border Biomedical Research Center, and Environmental Science and Engineering, University of Texas at El Paso, El Paso, Texas 79968, United States;* orcid.org/0000-0002-7954-0717; Email: xli4@utep.edu

Authors

Wan Zhou − *Department of Chemistry and Biochemistry, University of Texas at El Paso, El Paso, Texas 79968, United States;* orcid.org/0000-0002-1439-9548

Kaiqiang Hu − *Department of Chemistry and Biochemistry, University of Texas at El Paso, El Paso, Texas 79968, United States; College of Chemistry and Chemical Engineering, Qingdao University, Qingdao 266071, PR China*

Sharon Kwee − *Department of Biomedical and Chemical Engineering, University of Texas at San Antonio, San Antonio, Texas 78249, United States*

Liang Tang − *Department of Biomedical and Chemical Engineering, University of Texas at San Antonio, San Antonio, Texas 78249, United States*

Zonghua Wang − *College of Chemistry and Chemical Engineering, Qingdao University, Qingdao 266071, PR China;* orcid.org/0000-0002-9120-4089

Jianfei Xia − *College of Chemistry and Chemical Engineering, Qingdao University, Qingdao 266071, PR China*

Complete contact information is available at: https://pubs.acs.org/10.1021/acs.analchem.9b04996

Author Contributions

‡W.Z. and K.H. contributed equally.

https://dx.doi.org/10.1021/acs.analchem.9b04996
Anal. Chem. 2020, 92, 2739−2747

Notes

The authors declare no competing financial interest.

■ ACKNOWLEDGMENTS

We would like to acknowledge the financial support from the National Institute of Allergy and Infectious Disease of the NIH (R21AI107415), the U.S. NSF-PREM program (DMR 1827745), the Philadelphia Foundation, and the Medical Center of the Americas Foundation. Financial support from the National Institute of General Medical Sciences of the NIH (SC2GM105584), the NIH RCMI Pilot grant, University of Texas (UT) System for the STARS award, and the University of Texas at El Paso (UTEP) for the IDR Program, Multidisciplinary Research Award Program (MRAP) and URI Program is also greatly acknowledged. S.K. and L.T. thank the US. Department of Agriculture (2015-38422-24059) for partial support.

■ REFERENCES

(1) Dou, M.; Sanjay, S. T.; Dominguez, D. C.; Zhan, S.; Li, X. *Chem. Commun.* **2017**, *53*, 10886−10889.
(2) Dou, M.; Macias, N.; Shen, F.; Dien Bard, J.; Dominguez, D. C.; Li, X. J. *EClinicalMedicine* **2019**, *8*, 72−77.
(3) Xu, X. Y.; Wang, X. M.; Hu, J.; Gong, Y.; Wang, L.; Zhou, W.; Li, X. J.; Xu, F. *Electrophoresis* **2019**, *40*, 914−921.
(4) Wei, X. F.; Zhou, W.; Sanjay, S. T.; Zhang, J.; Jin, Q. J.; Xu, F.; Dominguez, D. C.; Li, X. J. *Anal. Chem.* **2018**, *90*, 9888−9896.
(5) Liu, P.; Li, X.; Greenspoon, S. A.; Scherer, J. R.; Mathies, R. A. *Lab Chip* **2011**, *11*, 1041−1048.
(6) Sanjay, S. T.; Zhou, W.; Dou, M. W.; Tavakoli, H.; Ma, L.; Xu, F.; Li, X. J. *Adv. Drug Delivery Rev.* **2018**, *128*, 3−28.
(7) Mangal, M.; Bansal, S.; Sharma, S. K.; Gupta, R. K. *Crit. Rev. Food Sci. Nutr.* **2016**, *56*, 1568−1584.
(8) Knopfmacher, O.; Hammock, M. L.; Appleton, A. L.; Schwartz, G.; Mei, J. G.; Lei, T.; Pei, J.; Bao, Z. N. *Nat. Commun.* **2014**, *5*, 2954.
(9) Xia, F.; Zuo, X. L.; Yang, R. Q.; Xiao, Y.; Kang, D.; Vallee-Belisle, A.; Gong, X.; Yuen, J. D.; Hsu, B. B. Y.; Heeger, A. J.; Plaxco, K. W. *Proc. Natl. Acad. Sci. U. S. A.* **2010**, *107*, 10837−10841.
(10) Zeng, Y.; Zhang, D.; Qi, P.; Zheng, L. B. *Microchim. Acta* **2017**, *184*, 4809−4815.
(11) Liu, P.; Yang, X. H.; Sun, S.; Wang, Q.; Wang, K. M.; Huang, J.; Liu, J. B.; He, L. L. *Anal. Chem.* **2013**, *85*, 7689−7695.
(12) Xu, W.; Xie, X. J.; Li, D. W.; Yang, Z. Q.; Li, T. H.; Liu, X. G. *Small* **2012**, *8*, 1846−1850.
(13) Bayrac, C.; Eyidogan, F.; Avni Oktem, H. *Biosens. Bioelectron.* **2017**, *98*, 22−28.
(14) Huang, J. H.; Ye, L.; Gao, X.; Li, H.; Xu, J. B.; Li, Z. G. *J. Mater. Chem. B* **2015**, *3*, 2395−2401.
(15) Liu, S. F.; Cheng, C. B.; Liu, T.; Wang, L.; Gong, H. W.; Li, F. *Biosens. Bioelectron.* **2015**, *63*, 99−104.
(16) Shi, J. Y.; Chan, C. Y.; Pang, Y. T.; Ye, W. W.; Tian, F.; Lyu, J.; Zhang, Y.; Yang, M. *Biosens. Bioelectron.* **2015**, *67*, 595−600.
(17) Dou, M. W.; Sanjay, S. T.; Dominguez, D. C.; Liu, P.; Xu, F.; Li, X. J. *Biosens. Bioelectron.* **2017**, *87*, 865−873.
(18) Zang, Y.; Lei, J. P.; Hao, Q.; Ju, H. X. *Biosens. Bioelectron.* **2016**, *77*, 557−564.
(19) Chen, J.; Qiu, H.; Zhang, M.; Gu, T.; Shao, S.; Huang, Y.; Zhao, S. *Biosens. Bioelectron.* **2015**, *68*, 550−555.
(20) Huang, H.; Bai, W.; Dong, C.; Guo, R.; Liu, Z. *Biosens. Bioelectron.* **2015**, *68*, 442−446.
(21) Cui, H. F.; Xu, T. B.; Sun, Y. L.; Zhou, A. W.; Cui, Y. H.; Liu, W.; Luong, J. H. T. *Anal. Chem.* **2015**, *87*, 1358−1365.
(22) Thiruppathiraja, C.; Kamatchiammal, S.; Adaikkappan, P.; Santhosh, D. J.; Alagar, M. *Anal. Biochem.* **2011**, *417*, 73−79.
(23) Deng, H.; Xu, Y.; Liu, Y. H.; Che, Z. J.; Guo, H. L.; Shan, S. X.; Sun, Y.; Liu, X. F.; Huang, K. Y.; Ma, X. W.; Wu, Y.; Liang, X. J. *Anal. Chem.* **2012**, *84*, 1253−1258.
(24) He, H. F.; Dai, J. Y.; Duan, Z. J.; Zheng, B. Z.; Meng, Y.; Guo, Y.; Xiao, D. *Sci. Rep.* **2016**, *6*, 30878.
(25) Dong, H.; Zou, F.; Hu, X.; Zhu, H.; Koh, K.; Chen, H. *Biosens. Bioelectron.* **2018**, *117*, 605−612.
(26) Hu, J.; Wang, L.; Li, F.; Han, Y. L.; Lin, M.; Lu, T. J.; Xu, F. *Lab Chip* **2013**, *13*, 4352−4357.
(27) Dou, M.; Dominguez, D. C.; Li, X.; Sanchez, J.; Scott, G. *Anal. Chem.* **2014**, *86*, 7978−7986.
(28) Dou, M.; Sanchez, J.; Tavakoli, H.; Gonzalez, J. E.; Sun, J.; Dien Bard, J.; Li, X. *Anal. Chim. Acta* **2019**, *1065*, 71−78.
(29) Zuo, P.; Li, X.; Dominguez, D. C.; Ye, B.-C. *Lab Chip* **2013**, *13*, 3921−3928.
(30) Katla, S. K.; Zhang, J.; Castro, E.; Bernal, R. A.; Li, X. *ACS Appl. Mater. Interfaces* **2018**, *10*, 75−82.
(31) Yu, Z.; Wang, M.; Pan, W.; Wang, H.; Li, N.; Tang, B. *Chem. Sci.* **2017**, *8*, 4896−4903.
(32) Zhang, T. T.; Xu, C. H.; Zhao, W.; Gu, Y.; Li, X. L.; Xu, J. J.; Chen, H. Y. *Chem. Sci.* **2018**, *9*, 6749−6757.
(33) Zhan, L.; Guo, S. Z.; Song, F.; Gong, Y.; Xu, F.; Boulware, D. R.; McAlpine, M. C.; Chan, W. C. W.; Bischof, J. C. *Nano Lett.* **2017**, *17*, 7207−7212.
(34) Gao, S.; Zhang, L. W.; Wang, G. H.; Yang, K.; Chen, M. L.; Tian, R.; Ma, Q. J.; Zhu, L. *Biomaterials* **2016**, *79*, 36−45.
(35) Chen, D. Q.; Wang, C.; Nie, X.; Li, S. M.; Li, R. M.; Guan, M. R.; Liu, Z.; Chen, C. Y.; Wang, C. R.; Shu, C. Y.; Wan, L. J. *Adv. Funct. Mater.* **2014**, *24*, 6621−6628.
(36) Ding, X.; Liu, J. H.; Li, J. Q.; Wang, F.; Wang, Y. H.; Song, S. Y.; Zhang, H. J. *Chem. Sci.* **2016**, *7*, 6695−6700.
(37) Li, X. S.; Peng, X. H.; Zheng, B. D.; Tang, J. L.; Zhao, Y. Y.; Zheng, B. Y.; Ke, M. R.; Huang, J. D. *Chem. Sci.* **2018**, *9*, 2098−2104.
(38) Fu, G. L.; Sanjay, S. T.; Li, X. J. *Analyst* **2016**, *141*, 3883−3889.
(39) Fu, G.; Sanjay, S. T.; Zhou, W.; Brekken, R. A.; Kirken, R. A.; Li, X. *Anal. Chem.* **2018**, *90*, 5930−5937.
(40) Fu, G. L.; Sanjay, S. T.; Dou, M. W.; Li, X. J. *Nanoscale* **2016**, *8*, 5422−5427.
(41) Sanjay, S. T.; Dou, M.; Sun, J.; Li, X. *Sci. Rep.* **2016**, *6*, 30474.
(42) Wu, H.; Bao, Y.; Wang, L.; Li, X.; Sun, J. *Int. Immunopharmacol.* **2019**, *73*, 41−48.
(43) Zhang, Q.; Wang, D. C.; Jiang, G. Z.; Liu, W.; Deng, Q.; Li, X. J.; Qian, W.; Ouellet, H.; Sun, J. *Sci. Rep.* **2016**, *6*, 32618.
(44) Pamies, R.; Cifre, J. G. H.; Espín, V. F.; Collado-González, M.; Baños, F. G. D.; de la Torre, J. G. *J. Nanopart. Res.* **2014**, *16*, 2376.
(45) Li, H.; Rothberg, L. *Proc. Natl. Acad. Sci. U. S. A.* **2004**, *101*, 14036−14039.
(46) Nelson, E. M.; Rothberg, L. J. *Langmuir* **2011**, *27*, 1770−1777.
(47) Carnerero, J. M.; Jimenez-Ruiz, A.; Grueso, E. M.; Prado-Gotor, R. *Phys. Chem. Chem. Phys.* **2017**, *19*, 16113−16123.
(48) Gopinath, S. C. B.; Lakshmipriya, T.; Awazu, K. *Biosens. Bioelectron.* **2014**, *51*, 115−123.
(49) Zhang, X.; Servos, M. R.; Liu, J. W. *Langmuir* **2012**, *28*, 3896−3902.
(50) Murphy, S. C. *Virtual Mentor.* **2006**, *8*, 245−250.
(51) Veigas, B.; Jacob, J. M.; Costa, M. N.; Santos, D. S.; Viveiros, M.; Inacio, J.; Martins, R.; Barquinha, P.; Fortunato, E.; Baptista, P. V. *Lab Chip* **2012**, *12*, 4802−4808.
(52) Hussain, M. M.; Samir, T. M.; Azzazy, H. M. *Clin. Biochem.* **2013**, *46*, 633−637.
(53) Torati, R.; Reddy, V.; Yoon, S. S.; Kim, C. *Biosens. Bioelectron.* **2016**, *78*, 483−488.
(54) Liu, D. Y.; Liang, G. T.; Zhang, Q.; Chen, B. *Anal. Chem.* **2013**, *85*, 4698−4704.
(55) He, Y.; Huang, G. M.; Cui, H. *ACS Appl. Mater. Interfaces* **2013**, *5*, 11336−11340.
(56) Ma, J. L.; Yin, B. C.; Le, H. N.; Ye, B. C. *ACS Appl. Mater. Interfaces* **2015**, *7*, 12856−12863.
(57) Tsai, T. T.; Shen, S. W.; Cheng, C. M.; Chen, C. F. *Sci. Technol. Adv. Mater.* **2013**, *14*, No. 044404.
(58) Zhang, C. L.; Xu, J.; Zhang, S. M.; Ji, X. H.; He, Z. K. *Chem. - Eur. J.* **2012**, *18*, 8296−8300.

https://dx.doi.org/10.1021/acs.analchem.9b04996
Anal. Chem. 2020, 92, 2739−2747

(59) Li, H. J.; Liu, F. Y.; Sun, S. G.; Wang, J. Y.; Li, Z. Y.; Mu, D. Z.; Qiao, B.; Peng, X. J. *J. Mater. Chem. B* **2013**, *1*, 4146−4151.
(60) Zhou, S. Y.; Zheng, W.; Chen, Z.; Tu, D. T.; Liu, Y. S.; Ma, E.; Li, R. F.; Zhu, H. M.; Huang, M. D.; Chen, X. Y. *Angew. Chem., Int. Ed.* **2014**, *53*, 12498−12502.
(61) Xia, F.; White, R. J.; Zuo, X.; Patterson, A.; Xiao, Y.; Kang, D.; Gong, X.; Plaxco, K. W.; Heeger, A. J. *J. Am. Chem. Soc.* **2010**, *132*, 14346−14348.
(62) Wei, X.; Wang, Y.; Zhao, Y.; Chen, Z. *Biosens. Bioelectron.* **2017**, *97*, 332−337.
(63) Li, Y.; Qi, X. D.; Lei, C. C.; Yue, Q. F.; Zhang, S. S. *Chem. Commun.* **2014**, *50*, 9907−9909.
(64) Yoo, S. M.; Lee, S. Y. *Trends Biotechnol.* **2016**, *34*, 7−25.
(65) Chung, C. H.; Kim, J. H.; Jung, J.; Chung, B. H. *Biosens. Bioelectron.* **2013**, *41*, 827−832.

https://dx.doi.org/10.1021/acs.analchem.9b04996
Anal. Chem. 2020, 92, 2739−2747